doi:10.26443/seismica.v4i2.2041

Earthquake relocations illuminate tectonics along the Bismarck Sea Seismic Lineation, Papua New Guinea

Anna M. Ledeczi *[1], **Göran Ekström** [2], **Brian Taylor** [3]

[1]Department of Earth and Space Sciences, University of Washington, Seattle, WA, [2]Lamont-Doherty Earth Observatory of Columbia University, Palisades, NY, [3]School of Ocean and Earth Science and Technology, University of Hawai'i at Manoa, Honolulu, HI

Author contributions: *Conceptualization*: G. Ekström. *Investigation*: A. Ledeczi. *Methodology*: A. Ledeczi, G. Ekström, B. Taylor. *Software*: G. Ekström. *Supervision*: G. Ekström, B. Taylor. *Visualization*: A. Ledeczi. *Writing – original draft*: A. Ledeczi. *Writing – review & editing*: A. Ledeczi. G. Ekström, B. Taylor.

Abstract The Bismarck Sea Seismic Lineation (BSSL) is a 1000-km-long band of shallow earthquakes that marks the boundaries between the North and South Bismarck Plates and the Manus Microplate, offshore Papua New Guinea. These tectonic boundaries comprise a series of transform faults separated by spreading ridges, and one extensional transform zone (ETZ). Since it was first identified in 1969, the deformation details of the faults along the BSSL have remained shrouded by the cloud of seismicity surrounding them. Here, we employ a recently published surface wave earthquake relocation algorithm (Howe et al., 2019) to relocate events along the BSSL and the previously proposed Adelbert block boundary. These relocations show that left-lateral strike-slip seismicity concentrates narrowly along the known transform faults (the Schouten, Willaumez, Djaul, and Weitin) and the western ETZ. Several events that relocate to inside the Manus Microplate may represent distributed deformation by right-lateral bookshelf-style faulting. The spreading ridges are aseismic at our scale of observation, as previously suggested, but we identify clusters of strike-slip events at their terminations. The strike-slip events along the ETZ are at synthetic Riedel shear angles of ~10° to those along the Willaumez transform. The earthquake relocations also show that the previously proposed SE boundary of the Adelbert block is not well defined or localized. We carefully selected the best quality relocated focal mechanisms to calculate new best-fit Euler poles for the transform segments. These calculations support earlier indications that the Schouten transform is not well fit by the same Euler pole as the other BSSL transforms, requiring internal deformation of the adjoining plates, for which we present additional evidence.

Non-technical summary When earthquakes occur, their signals are recorded by seismometers on land. However, in oceanic areas, these seismometers can be distant or sparse, resulting in a high level of earthquake location uncertainty. This uncertainty can pose an issue because many plate tectonic boundaries are identified based on earthquake locations. Here, we focus on earthquakes recorded along a series of faults known as the Bismarck Sea Seismic Lineation (BSSL) that separates the North Bismarck and South Bismarck Plates and Manus Microplate, offshore Papua New Guinea. We use seismic data to improve the locations of these earthquakes, showing that they occur on or near the known faults along this boundary. We then find best-fit poles of rotation that describe these fault segments and show that not all fault segments along this boundary can be well fit by the same pole, indicating some internal deformation of these plates and that not all deformation is accommodated at their boundaries.

Production Editor: Yen Joe Tan
Handling Editor: Matt Wei
Copy & Layout Editor: Théa Ragon

Received: October 8, 2025
Accepted: November 22, 2025
Published: December 8, 2025

1 Introduction

The deformation occurring between the obliquely and rapidly converging Pacific and Australian Plates is partitioned around a series of microplates that are relatively aseismic compared to the zones of intense earthquake seismicity that characterize their boundaries (e.g., Johnson and Molnar, 1972; Bird, 2003; Hasterok et al., 2022; Tregoning et al., 1999). The number of microplates and the nature of their boundaries continue to be investigated and revised (e.g., Wallace et al., 2004; Koulali et al., 2015; Benyshek et al., 2024).

One such boundary, between the North and South Bismarck Plates, is the Bismarck Sea Seismic Lineation (BSSL), a 1000-km-long band of shallow earthquakes that transects the Bismarck Sea, Papua New Guinea, from 143.5°E to 152.5°E between 3°S and 4°S (Fig. 1). Well located earthquake hypocenters and focal mechanisms are a necessary part of any tectonic interpretation of the BSSL. However, the location uncertainties for events in the Global Centroid Moment Tensor (GCMT) catalog, though improved from USGS values, are still on average 20 to 30 km (Dziewonski et al., 1981; Ekström et al., 2012; Smith and Ekström, 1996). As a result, the structures along the BSSL appear surrounded by a diffuse cloud of seismicity when plotting GCMT event locations (Fig. 1), and modern-day interpretations that rely on these hypocenters can lead to imprecise or misleading results.

To develop a clearer view of the seismically active structures along the BSSL, we apply the methods of

*Corresponding author: Anna Ledeczi (ledeczi@uw.edu)

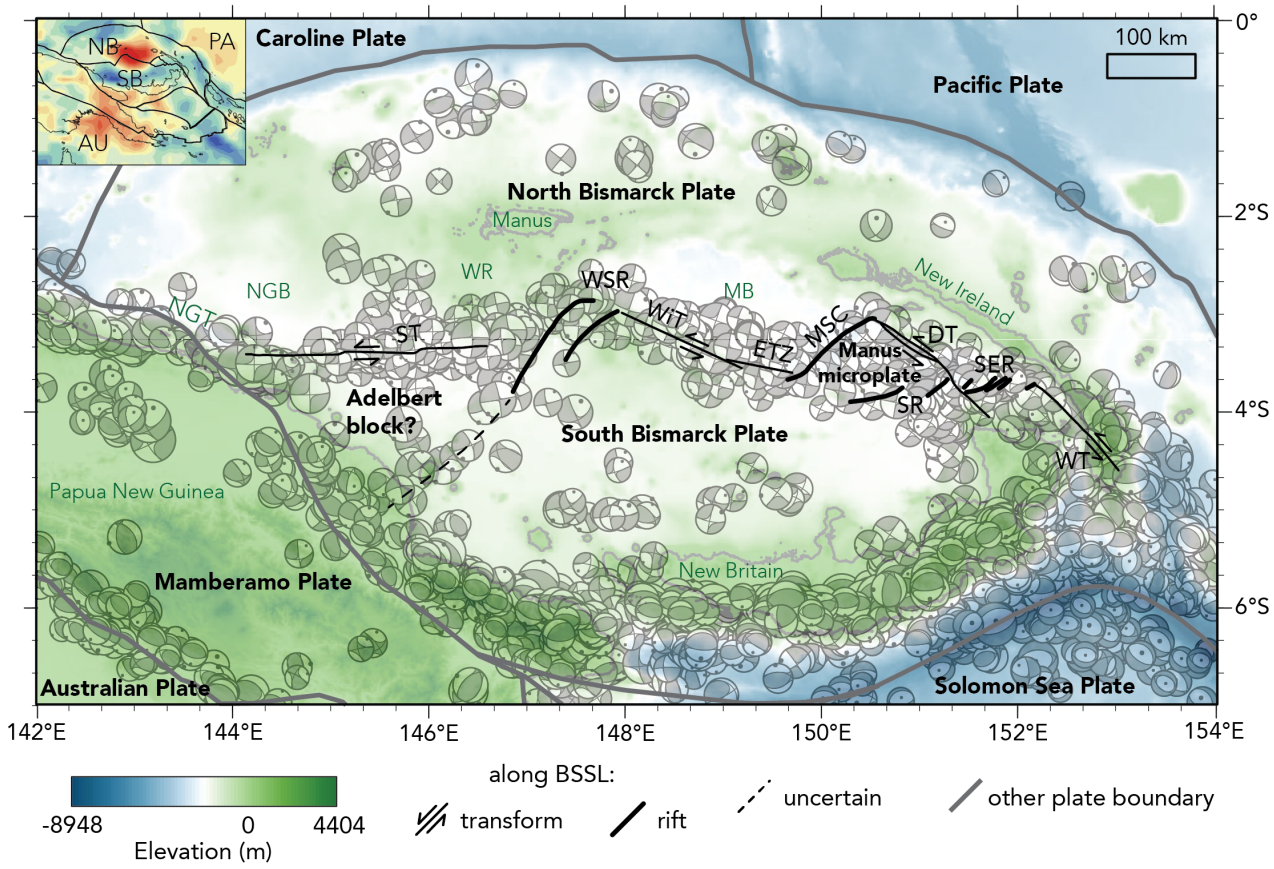

Figure 1 Tectonic and physiographic map of the BSSL. Regional plate boundaries surrounding the BSSL are adapted from Bird (2003), Hasterok et al. (2022), and Benyshek et al. (2024). Plate boundary segments of the BSSL include: ST: Schouten Transform, WSR: Western Spreading Ridges, WiT: Willaumez Transform, ETZ: Extensional Transform Zone, MSC: Manus Spreading Center, DT: Djaul Transform; SR, Southern Rifts, SER: Southeastern Ridges, WT: Weitin Transform. Other features: WR: Willaumez Rise, NGT: New Guinea Trench, NGB: New Guinea Basin, MB: Manus Basin. Bathymetry used here and in background of subsequent figures is from the GEBCO Bathymetric Compilation Group (2023). Focal mechanisms from the Global CMT Project (Dziewonski et al., 1981; Ekström et al., 2012). Inset: 500-km-depth slice of the UU-P07 P-wave velocity tomography that images the Manus plume (Hall and Spakman, 2002; Taylor and Benyshek, 2024). PA: Pacific, AU: Australia, NB: North Bismarck, SB: South Bismarck.

Howe et al. (2019), which use surface waves to relatively relocate groups of earthquakes with respect to each other, reducing location uncertainties from Global Seismographic Network values by a factor of ten or more. Our relocations reveal narrow bands of seismicity (few km wide) along the 100-to-200-km-long transform segments of the BSSL. Our relocations also confirm the aseismic behavior of the intervening spreading ridges, and identify strike-slip seismicity at their terminations. The small relocation uncertainties (average 3 km) allow us to calculate Euler poles of rotation that best fit the earthquake locations along the transform segments, individually and collectively. They confirm that the western (Schouten) transform is not well fit by Euler poles that describe the other BSSL segments well (Taylor, 1979). Oblique Mercator projections about the Euler poles show tight clustering of the GCMT slip vectors of the transform fault earthquakes along the best-fit-pole-predicted directions.

We discuss the implications of the Schouten transform not sharing the same pole as the other transforms of the BSSL. One proposal is that it forms the northern boundary of another block, the Adelbert block, separate from the South Bismarck Plate (Abers and McCaffrey, 1988; Koulali et al., 2015; Wallace et al., 2004). We relocated earthquakes along the proposed southeastern boundary of the Adelbert block to show that these events do not align into a narrow, well-defined zone. As an alternative, we present other evidence for internal deformation of the adjoining North and South Bismarck Plates.

1.1 History of Work on the Bismarck Sea Seismic Lineation

Denham (1969) first identified the BSSL based on earthquake hypocenter locations and, since it did not correspond to seafloor features then known, he chose the term 'lineation' to describe it. Johnson and Molnar (1972) determined left-lateral strike-slip focal mechanisms for three earthquakes aligned E-W along the western part of the BSSL and for three earthquakes aligned NW-SE in the east, and noted that the geologically young

left-lateral strike-slip fault that crosses the southern end of New Ireland (the Weitin River Fault, Brooks et al., 1971; Hohnen, 1970) may be an extension of the BSSL. They suggested that the BSSL represented a sinistral strike-slip fault that separated the largely aseismic North and South Bismarck Plates.

An Australian Bureau of Mineral Resources marine geophysical survey of the Bismarck Sea in 1970 acquired 40-50-km-spaced N-S profiles that documented the regional physiography and sediment distribution (Connelly, 1974, 1976; Taylor, 1975). A volcanic rise between Manus Island (on the northern remnant arc) and the Willaumez Peninsula of New Britain (a cross-chain of the southern active arc) separates the thickly sedimented New Guinea Basin in the west from the Manus Basin in the east (Fig. 1). A sediment-free zone across the center of the Manus Basin with normally-magnetized basement was recognized as a possible spreading center, though seemingly with some strikingly different characteristics to mid-ocean ridges (Connelly, 1976).

Further study showed that the earthquakes along the BSSL were too geographically scattered to represent a single strike-slip fault (Taylor, 1979; Ripper, 1975a,b) but instead comprised 100-200-km-long linear segments with left-lateral strike-slip focal mechanisms having one slip plane parallel to the strike of the segments. In addition to the Weitin fault, these segments included what came to be known as the Djaul, Willaumez and Schouten transform faults (Fig. 1). A Research Vessel (R/V) Vema 3313 profile collected sub-parallel to the bounding Willaumez and Djaul transforms allowed Taylor (1979) to model magnetic anomalies on the Manus spreading center back to 3.5 Ma, calculating a very fast total opening rate (132 mm/yr). He also concluded that the BSSL transform segments bounding the Manus Basin could not lie on small circles to the same pole of rotation as the Schouten transform to the west, which transects the New Guinea Basin; pure strike-slip motion (as suggested by the focal mechanisms) would require either that the largely aseismic North and South Bismarck Plates undergo significant internal deformation, or that the Schouten fault also undergoes a component of extension (at different times than its strike-slip faulting). Others have suggested that the Schouten transform could be a boundary between the Adelbert block and the North Bismarck Plate (Abers and McCaffrey, 1988; Koulali et al., 2015; Wallace et al., 2004). Meanwhile, the Willaumez Rise was associated with hot-spot volcanism in St. Andrew Strait (southeast of Manus Island, Johnson et al., 1978, 1979) above the Manus plume subsequently imaged by mantle P-wave-velocity tomography to extend from the surface to the core-mantle boundary (Fig. 1 inset, Taylor and Benyshek, 2024; Hall and Spakman, 2002).

Sidescan and underway geophysical profiling on R/V Moana Wave cruise 85-17 mapped the offshore Weitin, Djaul and Willaumez transforms and defined the intervening extensional zones, including the Southeast Ridges, Southern Rifts, Manus Spreading Center, and Extensional Transform Zone (ETZ; Fig. 1; Taylor et al., 1986, 1991). The Manus ETZ was categorized as a new type of plate boundary accommodating oblique spreading on overlapping, en echelon volcanic zones cut by faults oriented at Riedel shear angles of 10° to 15° synthetic to the Willaumez transform. Comparable structures were later recognized globally in the Lau Basin, Reykjanes Peninsula and Mak'Arrasou Afar (Taylor et al., 1994; Zellmer and Taylor, 2001). A one-month deployment of an array of eight ocean bottom seismometers showed that the left-lateral earthquakes on the Willaumez transform and the Riedel shear of the ETZ had a very narrow distribution (few km wide) and that the volcanic zones were aseismic (Eguchi et al., 1986, 1989a). Spreading rates increasing SW along the Manus Spreading Center were interpreted to be complemented by rifting rates increasing to the NE along the Southern Rifts, with a counter-clockwise-rotating Manus microplate in between (Martinez and Taylor, 1996, 2003).

The neovolcanic zones identified on R/V Moana Wave cruise 85-17 were extensively sampled on the following cruise 85-18, allowing the identification of diverse mid-ocean ridge and H_2O-rich back-arc basin basalt types on the Manus Spreading Center and ETZ, with the high radiogenic helium signature of a mantle plume (Macpherson et al., 1998; Sinton, 2003; Sinton et al., 1986). Some accompanying bottom photographs led to the discovery of the first massive sulfide chimneys in the western Pacific, along with their distinctive gastropod vent macrofauna (Both et al., 1986). This discovery was followed by many international research cruises to study the hydrothermal activity, including ODP Leg 193 (Auzende et al., 1996, 2000; Barriga et al., 2007; Binns and Scott, 1993; Crook et al., 1997; Tufar, 1990). Of these cruises, those by the Metal Mining Agency of Japan and the Institut Français de Recherche pour l'Exploitation de la Mer were most important in further defining the BSSL in that they swath mapped what has been collectively termed the (overlapping) Western Spreading Ridges and the eastern Schouten transform fault (Fig. 1, see summary in Lee and Ruellan, 2006). The westernmost segment of the BSSL, named the Schouten fault after the island arc volcanoes it transects, was swath mapped with sidescan and bathymetry and acoustic imagery on R/V Kilo Moana cruise KM0419 (Llanes et al., 2009). The seafloor traces of the Schouten fault are oriented E-W, with local restraining and releasing bends, and may continue onshore in a series of anastomosing faults along the northern coastal ranges of New Guinea that accommodate some of the sinistral component of oblique convergence across the easternmost New Guinea Trench (Fig. 1, Cooper and Taylor, 1987). In all, the four principal transform fault segments and intervening spreading segments of the BSSL have been completely swath mapped, with the exception of the central segment of the Schouten fault from 145.15°E-145.5°E. Crustal motion surveys using campaign GPS have confirmed the rapid relative motion of the microplates in the region (Fig. 1 inset, Bird, 2003), including sinistral motion along the BSSL (Koulali et al., 2015; McClusky et al., 1994; Tregoning, 2002; Wallace et al., 2004).

Segment	Date range	Min. Mw	Max. Mw	Starting events (n)	Relocated events (n)	Average uncertainty (km)	Euler pole calculation events (n)	Average uncertainty (km)
Schouten	2004/01/01 to 2023/12/31	4.7	6.6	137	137	3.00	76	2.82
Willaumez	2004/01/01 to 2023/12/31	4.7	6.4	156	154	2.98	45	1.85
Djaul, Manus SR1, & SER2	2004/01/01 to 2023/12/31	4.7	6.3	114	114	2.93	39	2.22
Weitin	2000/01/01 to 2023/12/31	5.0	7.7	24	19	4.91	6	3.23
Adelbert	1976/01/01 to 2023/12/31	5.3	6.4	28	9	8.41		

Table 1 Inversion parameters and results. Events successfully relocated in the initial inversion are all events with depth less than 50 km that relocate with uncertainty less than 10 km. Events for the Euler pole calculation are selected by procedures detailed in the methods.

2 Data and Methods

Our objective was to determine better locations for a representative sample of earthquakes along the BSSL in order to refine the characterization of the plate boundary. We selected earthquakes based on location, magnitude, and the existence of a moment tensor result in the Global CMT (GCMT) catalog. The GCMT catalog is nearly complete for earthquakes Mw ≥ 5.0 globally starting in 2004. To determine better locations for the events, we use the surface-wave-relocation method of Howe et al. (2019). In this approach, which is similar to that of Cleveland and Ammon (2013), cross correlation of intermediate-period surface waves recorded at teleseismic distances is used to determine relative travel times for pairs of earthquakes in a cluster of earthquakes. Travel-time differences for all pairs of earthquakes in the cluster are then inverted simultaneously to determine a set of relative locations that best predict the observed travel-time differences. The method is analogous to the more commonly used joint-hypocenter determination and double-difference method used to improve relative locations using body-wave phases.

Rayleigh and Love waves in the period band 30–80 s at common stations are correlated at stations recording both of the earthquakes in a pair of events. Multiple subsets of the travel-time data are inverted separately to estimate realistic errors in the resulting locations. The uncertainties that encompass the locations from all the subsamples are displayed as ellipses around the final location, of which the length in km of the semimajor axis is used to quantify the uncertainty. If an area involves a mix of focal mechanisms, increased uncertainty can be introduced into the relocation for which Howe et al. (2019) apply a source correction. This source correction is not applied here because we investigated transform segments with almost exclusively strike-slip mechanisms for which we do not expect the source correction to significantly reduce uncertainty, as seen when applied to the Blanco and Balleny transform fault zones by Howe et al. (2019). We used the slowness predicted by the global reference model PREM (Dziewonski and Anderson, 1981) to convert the measured differential travel times to differential distances; however, since interevent distances are short, varying the slownesses does not appreciably change the relative locations of the events. All events in this study are constrained by more than 300 independent differential travel times. If the azimuthal coverage for a given event is not adequate, this will increase the location uncertainties; thus, events with inadequate azimuthal coverage are filtered out during the subsequent steps.

Since the algorithm solves only for improved relative locations, no improvement in the absolute location of the cluster is obtained. The centroid of the cluster locations is therefore held fixed in the inversion, and other methods, such as alignment with known structures, can be used to reference the cluster geographically. We use published bathymetry and other seafloor data to map in detail the structures associated with the BSSL. In areas where the relocations align with one of these segments, we perform a final translation of the earthquake epicenters to match these boundaries. This is viable because the strike-slip focal mechanisms show that the dip of the faults are very close to vertical. In regions where much of the deformation may be distributed, diffuse, or unconstrained, this final step is not performed.

We collected long-period digital seismograms from the Global Seismographic Network (Albuquerque Seismological Laboratory/USGS, 1988; EarthScope Consortium, 1986), Geoscope (Institut de physique du globe de Paris (IPGP) and École et Observatoire des sciences de la Terre de Strasbourg (EOST), 1982), GEOFON (GEOFON Data Centre, 1993), and MedNet (MedNet Project Partner Institutions, 1990) seismic networks and from a few additional stations from regional networks. Typically, data from around 200 globally distributed stations are available for each earthquake. Smaller earthquakes

(around Mw 5) may only record good surface-wave signals on a small subset of the stations. We correlated the surface waves for all event pairs with an interevent separation smaller than 200 km, and only considered traveltime observations with a cross-correlation coefficient greater than 0.9 in the inversion. We relocated events in sections of 3.5° in longitude and smaller to minimize any errors that heterogeneities in shallow earth structure over longer distances may introduce. Horizontal-location uncertainties can be influenced by the number of earthquakes, area of analysis, or mix of focal mechanisms, which can impact the quality of the relocations. We relocated subsamples of the earthquakes with replacement and determine how the location of each individual event is impacted. Horizontal location uncertainties from this process are reported as ellipses and we exclude any events that relocate with an uncertainty greater than 10 km on the semimajor axis.

Throughout the study area, we first chose events with Mw>4.5 and a centroid depth shallower than 50 km. Our initial selection of events along the Schouten transform (Fig. 2), Willaumez transform (Fig. 3), and Manus microplate (Fig. 4) includes all events in the GCMT catalog for the period 2004/01/01 to 2023/12/31 that are located between 2.8°S and 4.0°S, 143.9°E and 147.2°E; 2.6°S and 4.2°S, 147.2°E and 150.1°E; and 3.0°S and 4.4°S, 149.7°E and 152.2°E, respectively (Table 1). For the Weitin transform (Fig. 4), we selected earthquakes from 2000/01/01 through 2023/12/31, in the geographic region 3.6°S to 4.8°S, 152.2°E to 153.4°E, to capture two notable events, the 2000 Mw 8.0 and 2019 Mw 7.7 (see e.g., Chen et al., 2019). Because the Adelbert block region (Fig. 5) has fewer earthquakes, we used a longer period of observation from 1976/01/01 through 2023/12/31 within the area 3.5°S and 5.0°S, 145.4°E and 147.2°E. These criteria lead to the identification of events shown in Table 1. The majority of relocated events fall near the BSSL and have the expected left-lateral strike-slip mechanisms. We show all events that successfully relocated with horizontal-location uncertainties less than 10 km and depth less than 50 km in each region, and display focal mechanisms scaled by magnitude listed in Table 1.

When calculating new best-fitting Euler poles, we carefully selected events that we believe are likely to represent the motion along the BSSL. We excluded events that relocate to greater than 10 km away from the fault and those that are not left-lateral strike-slip events, which may not represent motion on these specific fault structures. We calculated the strike of the closer nodal-plane of each event and eliminated those that are greater than 15° away from the median of each fault segment. We also excluded events from clusters that align at different azimuths compared to the mapped faults (e.g., cluster at 3.3°S, 146.9°E in Fig. 2). Finally, we removed all events bordering the Manus microplate, such as along the Djaul transform, as these represent motion other than that strictly between the North and South Bismarck Plates. We report the resulting number of events and their uncertainties in Table 1.

We compared the locations of the earthquakes associated with the different transform segments to those predicted by a relative plate-motion pole. On each segment, we assumed the earthquakes lie on a small circle defined by an Euler pole. Euler poles were calculated by minimizing the root-mean-square error (RMS) of the angular distance Δ between the relocated events and the predicted location from all possible Euler poles by solving

$$\cos\Delta = \sin\lambda_e \sin\lambda_p + \cos\lambda_e \cos\lambda_p \cos(\phi_e - \phi_p) \quad (1)$$

where (λ_p, ϕ_p) and (λ_e, ϕ_e) are the latitude and longitude of the test Euler pole and each relocated earthquake, respectively. We conducted a grid search across all possible latitude and longitude combinations at 0.1° increments. When fitting Euler poles to plate boundaries representing multiple fault segments, we performed this calculation for each segment separately, then weighted the RMS values by the number of earthquakes along each segment. We then performed bootstrapping, or sampling with replacement, 1000 times on the earthquake locations and recalculated the pole to derive a 95% confidence region for the pole locations.

Once these best-fit Euler poles had been chosen, we used oblique Mercator projections about the best-fit Euler poles to evaluate their validity. A correct pole turns fault segments into linear, east-west striking segments (i.e., lines of latitude in the oblique Mercator projection), and thus produces slip vectors oriented at 90-270° (see e.g., Joseph et al., 1993). These projections allowed us to confirm whether the poles calculated using the relocated earthquake locations are correct, since the Euler pole calculation itself does not take the slip vectors into account and is thus an independent assessment. Finally, given these Euler poles, we calibrated the angular velocities to estimates of rotation rates obtained from campaign GPS data in Tregoning (2002) and Koulali et al. (2015).

3 Results

3.1 Earthquake relocations

3.1.1 The Schouten transform

The trace of the Schouten transform was mapped from swath bathymetry of Llanes et al. (2009) in the west and of Auzende et al. (2000) in the east, with an intervening middle section from 145.15°E to 145.5°E with no high-resolution seafloor imagery. We relocated 137 events with less than 10 km uncertainty and applied a 0.05° shift to the north to align the events with the fault trace (Fig. 2a). The average uncertainty is 3.0 km for the successfully relocated events (Fig. 2b). In each region, relocation results without any removed events or seafloor alignment shifts can be found in the Supplemental Material (Ledeczi et al., 2025).

After relocation, the earthquake locations collapsed from a diffuse cloud down to a narrow, linear cluster of events that closely follow the mapped fault trace to within their average uncertainty. The events have primarily left-lateral strike-slip motion, with a few oblique reverse mechanisms at the western end of the Schouten, and no normal mechanisms. The Schouten has two ~2 km long extensional relays at 145.1 and

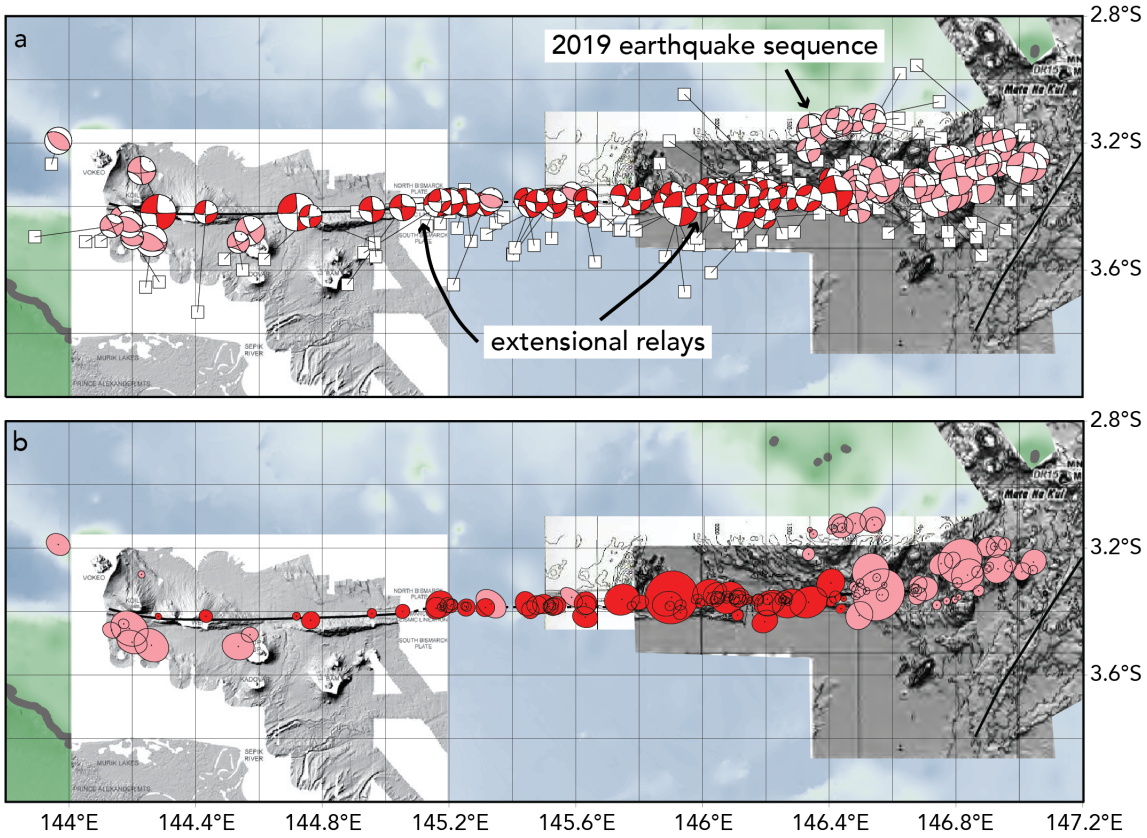

Figure 2 Relocated earthquakes along the Schouten transform. **a**. Events shown before (square) and after (focal mechanism) relocation. The size of the focal mechanism is proportional to the moment magnitude, which varies between Mw=4.7 and Mw=6.6. Locations of the 2019 earthquake sequence and extensional relays of the Schouten are indicated. **b**. Associated horizontal-location uncertainty ellipses represent a geographic area of uncertainty at the scale of the map throughout this manuscript. Red events are those included in pole calculations and pink events are excluded.

145.95°E which are reflected in the relocation of the events. Events east of 146.45°E show a rotation in the strike of the cluster of events, as well as a less linear alignment, which we interpret is due to interaction between strike-slip motion on the Schouten and spreading on known nearby ridges. Clustered just north of the Schouten near 3.2°S, 146.5°E, our relocations document a sequence of 11 earthquakes that occurred in January through March of 2019, during which no other events on the Schouten occurred. These events occurred in an area with no high-resolution bathymetry, but close to and at a similar trend to nearby bathymetric ridges.

For our Euler pole calculation, we selected 76 events as being strike-slip events occurring strictly on the Schouten following the criteria described in the methods. We excluded the aforementioned 2019 sequence and the events close to the Western Spreading Ridges. To better fit the relocated earthquakes, we calculated the Euler pole using three small circles at different distances separated by the two extensional relays described above. The average uncertainty of these events is 2.82 km; the reported RMS error, defined as the average of the three segments weighted by the number of events on each, is 1.58 km (Table 2).

3.1.2 The Willaumez transform and the ETZ

We mapped the traces of the Western Spreading Ridges with swath bathymetry from Auzende et al. (2000) and the Willaumez transform fault, ETZ, and Manus Spreading Center with acoustic imagery from Taylor et al. (1994). Out of 156 events, 154 are relocated with a location uncertainty smaller than 10 km. We applied a static shift of 0.05° to the south in order to align the locations with the bathymetric fault trace (Fig. 3a). The successfully relocated events on Fig. 3 have an average uncertainty of 2.98 km (Fig. 3b). The earthquakes all have left-lateral strike-slip mechanisms.

All the events between 148.1-149.0°E relocated onto the Willaumez as a narrow curvilinear band bearing 109° in the west to 115° in the east, parallel to the strike of their slip planes (Fig. 3). Farther west a cluster of 32 events occurs in two bands bearing 100°, the majority between the overlapping spreading segments of the Western Spreading Ridges and a handful farther north across the eastern spreading segment and towards the Willaumez transform. This cluster of events does not occur in a specific time period, like the sequence north of the Schouten, but throughout the period of study. Meanwhile, the spreading ridges themselves are aseismic, as an OBS study of the ETZ indicated (Eguchi et al.,

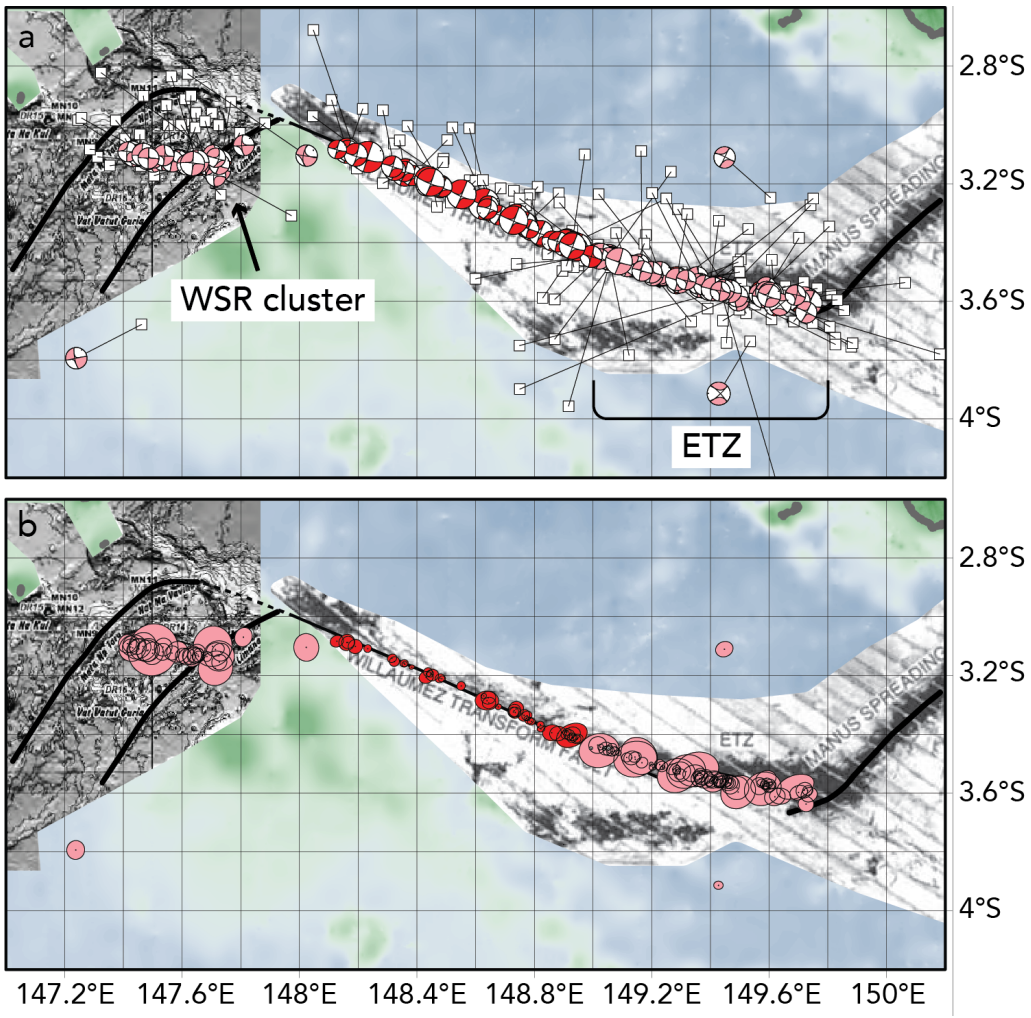

Figure 3 Relocated earthquakes along the Willaumez transform. **a**. Events shown before (square) and after (focal mechanism) relocation. The size of the focal mechanism is proportional to the moment magnitude, which varies between Mw=4.7 and Mw=6.4. WSR: Western Spreading Ridges. **b**. Associated horizontal-location uncertainty ellipses. Red events are those included in pole calculations and pink events are excluded.

1986). Events on the ETZ include a linear band bearing 106° from 149.0°E to 149.5°E, parallel to their slip planes, consistent with the Riedel shear interpretation of Taylor et al. (1994). Where the ETZ overlaps with the southwest end of the Manus Spreading Center, from 149.5-149.8°E, the seismicity zone widens and includes slip planes parallel to both the transform and to the Riedel shear. Two isolated strike-slip events occur north and south of the ETZ near 149.4°E. We included events only on the Willaumez for our Euler pole calculation, excluding both the WSR clusters and events along the ETZ. The remaining events have a small location uncertainty of 1.85 km.

3.1.3 The Djaul and Weitin transforms

We mapped the trace of the Djaul transform, Manus microplate, and Southern Rifts with sidescan imagery from Taylor et al. (1994); the Southeast Ridges with swath bathymetry from Auzende et al. (2000); and the Weitin transform from Taylor et al. (1991) and the surface ruptures detailed in Chen et al. (2019). We performed two separate inversions, one for the Djaul, Manus, and Southeast Ridges area, and one for the Weitin transform area, for higher precision over a large longitude range, but plotted all events on Fig. 4. For the Manus microplate and Southeast Ridges areas, 114 events were successfully relocated with < 10 km of uncertainty and a 0.05° northward static shift was applied. The majority of these events have strike-slip focal mechanisms, but there are a few normal and reverse faulting events. The cloud of seismicity around the Manus microplate shown in Fig. 1 collapses down to linear, narrow left-lateral strike-slip features, primarily along the Djaul transform (Fig. 4). However, the interior of the Manus Microplate also hosts seismicity. While both the Southern Rifts and Southeast Ridges themselves appear aseismic, there is a cluster of events at the end of each ridge. To calculate the NB/SB Euler pole, we excluded most of the events from this inversion. While the Djaul is technically part of the BSSL, since it is the boundary of the Manus microplate, these earthquakes may not reflect motion between the North and South Bismarck Plates. We did include two small clusters of strike-slip events, one between the Southern Rifts and Southeast Ridges the other between two of the Southeast Ridges, totaling 27 and 12 events with 2.04 and 2.64 km uncertainties, respectively (in Fig. 4a "SR1" and "SER2").

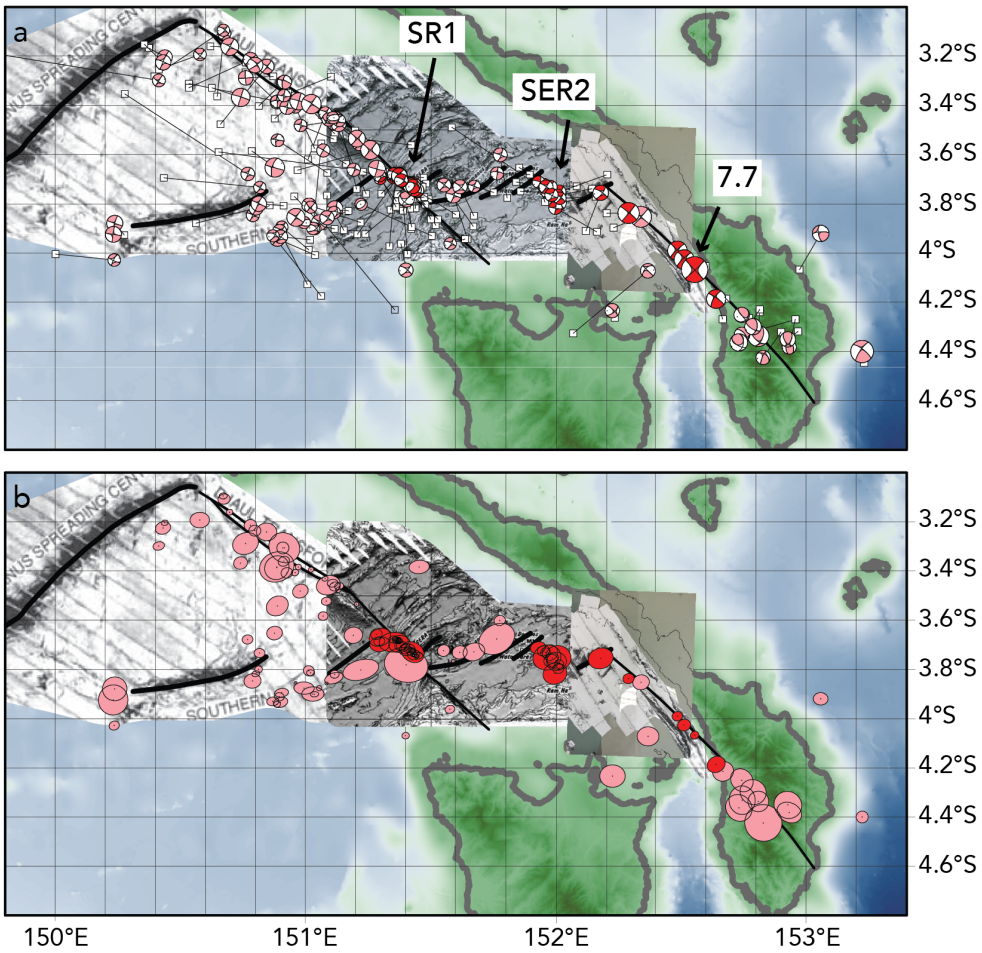

Figure 4 Two separate earthquake relocations, one along the Djaul transform and Southeastern Ridges area, and one for the Weitin transform, are shown in this figure. **a.** Events shown before (square) and after (focal mechanism) relocation. The size of the focal mechanism is proportional to the moment magnitude, which varies between Mw=4.7 and Mw=7.7. **b**. Associated horizontal-location uncertainty ellipses. Red events are those included in pole calculations and pink events are excluded.

The New Ireland region has many reverse-faulting earthquakes resulting from subduction of the Solomon Sea Plate beneath New Britain (Fig. 1). Once excluding all events deeper than 50 km, which are largely associated with the subducting slab, 19 events relocated in the Weitin region (Fig. 4). We applied a 0.06° shift to the south to this inversion to align the relocated events with the mapped fault trace. Many of the remaining earthquakes have reverse-faulting mechanisms, which we excluded. In addition, removing all events >10 km away from the Weitin fault and events with nodal-plane strikes greater than 15° away from the average leaves just 6 events that relocate with an average uncertainty of 3.23 km for the Euler pole calculation. We included these 6 events despite their slightly lower quality to get a larger longitude range to constrain our Euler pole calculations. The 2019 Mw 7.7 event successfully relocated and is used in our final Euler pole calculation. However, the 2000 Mw 8.0 earthquake was excluded because of its larger uncertainty of 13.2 km, which is likely because its fault slip ruptured at minimum the entire length of the Weitin fault exposed on land (61 km; Chen et al., 2019), and thus it is not well characterized by relocation to a point.

3.1.4 The Adelbert block

We relocated events along the proposed SE boundary of the Adelbert block (Abers and McCaffrey, 1988; Koulali et al., 2015; Wallace et al., 2004). There is little high-resolution seafloor imagery in this area except a few tracks of multibeam bathymetry from Lee and Ruellan (2006) shown in Fig. 5, making it difficult to determine whether there are any continuous seafloor fault traces in this region. Once excluding all deep seismicity and earthquakes far from the region of interest, only 9 events relocate with a location uncertainty smaller than 10 km. The average location uncertainty is high at 8.41 km (Table 1). These strike-slip earthquakes have left-lateral mechanisms relative to their NE- to ENE-nodal-planes, with T-axes almost orthogonal to their location trend of ~040° (Fig. 5). Having no seafloor imagery constraints, we neither apply a static shift of the events nor exclude any due to distance from the fault. There is a short lineation in the bathymetry near 4.0°S, 146.4°E that aligns well with the earthquake slip planes and could be a fault scarp, but the relocated earthquakes do not cluster there (Fig. 5a).

Source	Euler pole	σ_{maj} (°)	σ_{min} (°)	Azimuth (°)	ω (°/Myr)	RMS misfit with Schouten (km)	Overall RMS misfit (km)
Martinez and Taylor (1996) (NB/SB)	-11.0, 145.0	N/A	N/A	N/A	5.4	2.64	1.97
Tregoning (2002) (NB/SB)	-10.2, 146.5	0.2	0.1	7	8.75	3.32	2.94
Wallace et al. (2004) (NB/SB)	-10.45, 146.0	1.26	0.30	281.7	8.29	2.35	2.10
Koulali et al. (2015) (NB/SB)	-10.4, 146.6	N/A	N/A	N/A	8.65	3.47	3.17
This study, all BSSL (NB/SB)	-10.5, 145.5	0.49	0.07	199.7	7.85	2.07	1.66
This study, Willaumez, SER, and Weitin (WSW)	-13.2, 144.2	3.07	0.09	204.1	6.02	N/A	1.18
This study, Schouten only	-64.9, 146.3	56.32	3.16	180.1	1.41	1.58	1.58

Table 2 Published and newly calculated Euler poles and associated error ellipses and RMS misfit to the relocated earthquakes. RMS misfit over multiple segments is calculated separately and then weighted by the number of earthquakes per segment to get an average value

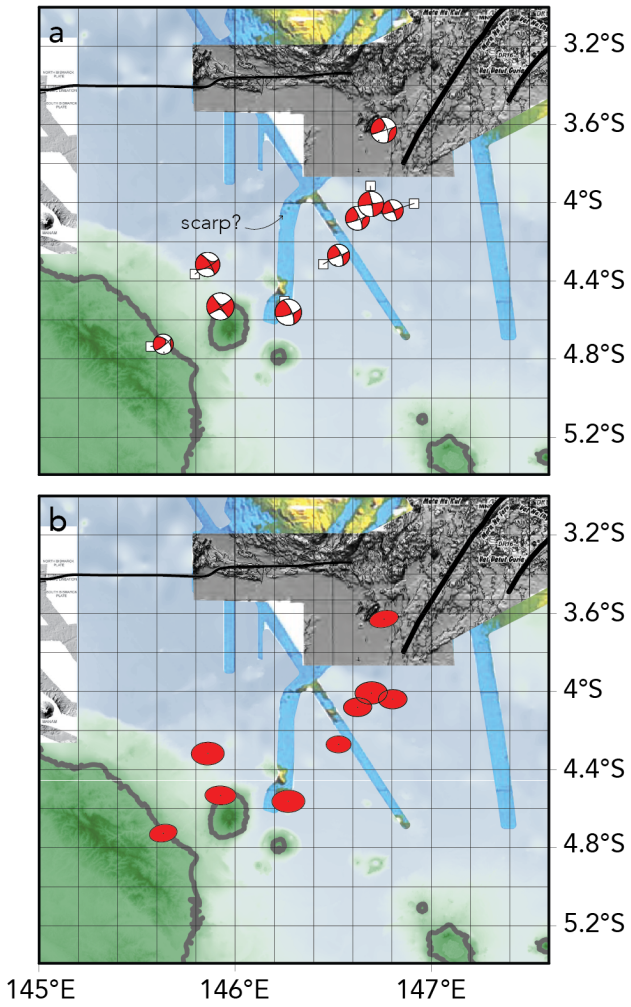

Figure 5 Relocated earthquakes along the proposed Adelbert block boundary. **a.** Events shown before (square) and after (focal mechanism) relocation. The size of the focal mechanism is proportional to the moment magnitude, which varies between Mw=5.3 and Mw=6.4. **b**. Associated horizontal-location uncertainty ellipses. Red events are all events which relocated along this boundary, but none are included in the pole calculation. There is a short lineation in the bathymetry near 4.0°S, 146.4°E which may be a fault scarp.

3.2 Euler pole calculations

Several Euler poles that describe the relative motion between the North and South Bismarck Plates have been published; all lie between -10.2° and -11°, 145° and 146.6° (Table 2). Previous work has also found that the Schouten transform is not well fit with the same Euler pole as the other segments of the BSSL (Taylor, 1979). We used the locations of the earthquakes and small circle predictions from the various poles to calculate an RMS misfit associated with each pole location, assuming that the earthquakes all lie on a single small circle. Finally, we calculated new best-fit Euler poles for the BSSL. To assess these newly calculated poles, we projected the slip vectors of the focal mechanisms about the best-fit Euler poles using oblique Mercator projections.

Our calculations show that the small circle paths associated with published Euler poles fit the relocated earthquakes along the Schouten worse than the BSSL as a whole and any other segment individually (Table 1). Of the published Euler poles, that of Wallace et al. (2004) has the lowest RMS misfit between the predicted small circle locations and the relocated earthquakes for both Schouten (2.35 km) and the entire BSSL (2.10 km). We calculated a new Euler pole for the entire BSSL of (-10.5°, 145.5°) (Fig. 6). We calibrated the predicted relative motion rates along the BSSL from Tregoning (2002) to our new pole and derived an angular rate of 7.85°/Myr. While this newly calculated pole does overlap with the confidence region of the pole of Wallace et al. (2005), it is significantly different from the Euler pole reported in Tregoning (2002) and that of Koulali et al. (2015), though the latter does not report an error ellipse (Fig. 7).

The small circles associated with this new Euler pole have a lower total RMS misfit to the earthquake locations along the entire BSSL of 1.66 km. However, the RMS misfit for the Schouten earthquake locations is higher than average at 2.07 km. The Schouten misfit is visible in Fig. 6, where both the eastern and western ends of the small circle predicted by the BSSL pole are misaligned with the earthquake locations and slip azimuths.

The inability of a given small circle to fit the earthquake locations is evident when using an oblique Mercator projection (OMP) about the calculated Euler pole,

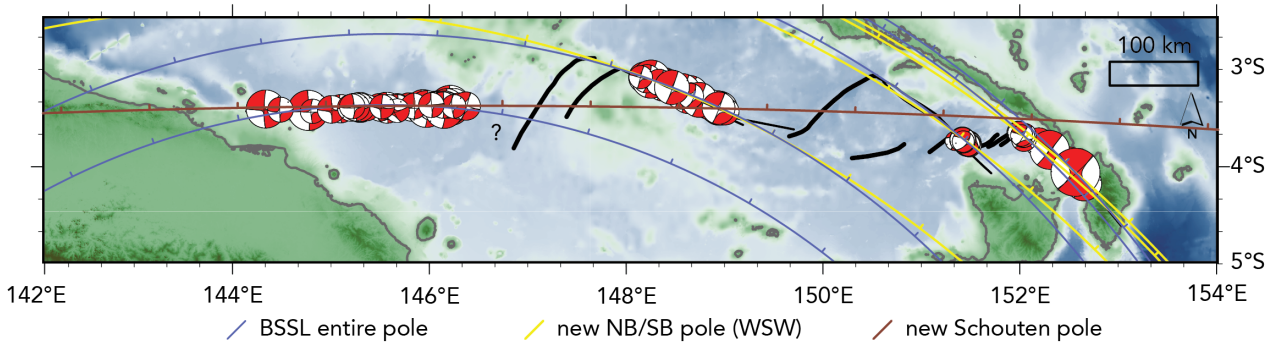

Figure 6 Events selected for inclusion in Euler pole calculations along the whole BSSL. Small circles are drawn at varying distances from the calculated poles.

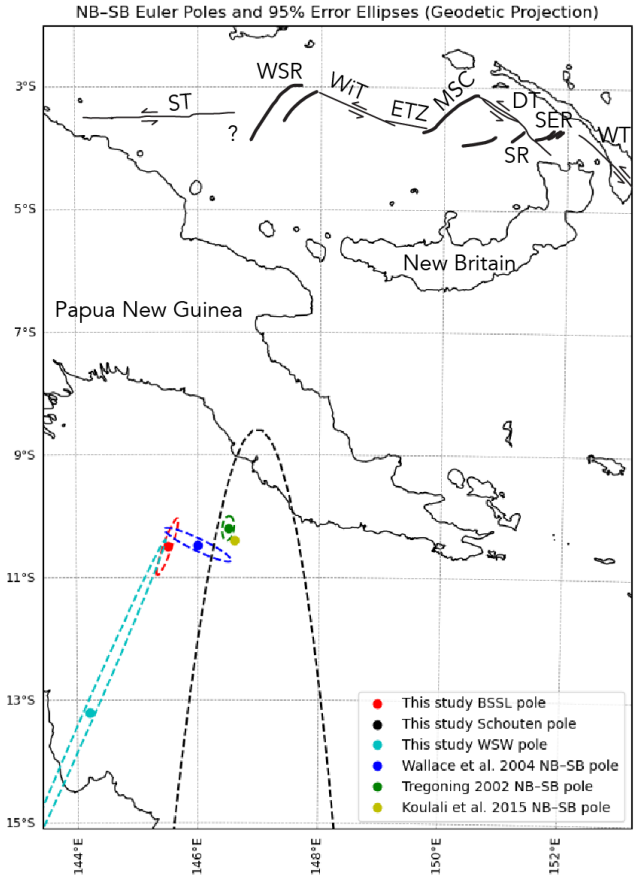

Figure 7 Previously published and newly calculated Euler poles and error ellipses. The Schouten Euler pole lies outside the map and only a portion of its 95% error ellipse is shown. Parameters for Euler poles are from Table 2. Plate boundary segments of the BSSL include ST: Schouten Transform, WSR: Western Spreading Ridges, WiT: Willaumez Transform, ETZ: Extensional Transform Zone, MSC: Manus Spreading Center, DT: Djaul Transform; SR, Southern Rifts, SER: Southeastern Ridges, WT: Weitin Transform.

where a correct pole should turn curved transforms into linear east-west striking segments. When applying our newly calculated BSSL Euler pole, the Schouten transform becomes curved (Fig. 8a). We used rose diagrams to display the projected strikes of the earthquake nodal-planes to evaluate whether the predicted small circles fit the earthquakes. Correctly fit events should plot at 90-270° since each OMP turns curved transforms into east-west striking segments. Along the Schouten, only about half of the selected and excluded events are well fit with the BSSL Euler pole, while the remainder plot ~10° anticlockwise, showing a systematic misfit (Fig. 8b). Meanwhile, the strikes of the nodal-planes along the Willaumez, Djaul, and Weitin plot close to 90 or 270° (Fig. 8c-e). The majority of both the Western Spreading Ridges cluster and the ETZ nodal-plane strikes plot in the 80 or 260° bin, showing a systematic ~10° anticlockwise rotation from east-west (Fig. 8c). Additionally, most of the nodal-plane strikes along the selected Southern Rifts and Southeast Ridges segments between the spreading ridges also appear to not align with the predicted small circles, instead showing the same 10° anticlockwise rotation (Fig. 8d).

Calculating an Euler pole for the segments without Schouten (Willaumez, Southern Rifts and Southeast Ridges, and Weitin, hereafter "WSW") gives a value of (-13.2°, 144.2°), where the predicted small circles and the earthquake locations have a reduced overall RMS misfit of 1.18 km (Table 1, Fig. 6). We calibrated the predicted relative motion rates along the eastern BSSL (i.e., excluding Schouten) from Tregoning (2002) to our new pole, deriving an angular rate of 6.02°/Myr. The exclusion of events along the Schouten causes the 95% confidence region to expand (Table 2); however, it does not overlap with that of our newly calculated BSSL pole (Fig. 7). The corresponding OMP (Fig. 8f) shows a similar pattern to that of the overall BSSL Euler pole, with a curved Schouten transform and linear segments otherwise. Notably, the rose diagrams show that the WSW Euler pole projection places more of the nodal-plane strikes in Southern Rifts, Southeast Ridges, and Weitin in the 90 or 270° bin (Fig. 8i) compared to the BSSL Euler pole. However, there is a roughly equal number of nodal-plane strikes along the Djaul (Fig. 8i-j), and slightly fewer along the Willaumez (Fig. 8h), at 90 or 270°. With Schouten events excluded from this calculation, the OMP plot shows that an Euler pole that fits the remainder of the segments well, causes almost none of the Schouten nodal-plane strikes to be fit correctly, instead most nodal-plane strikes plot at 80 or 260° (Fig. 8g). If these fault segments were copolar, the slip vectors of the relocated events along the Schouten would be ex-

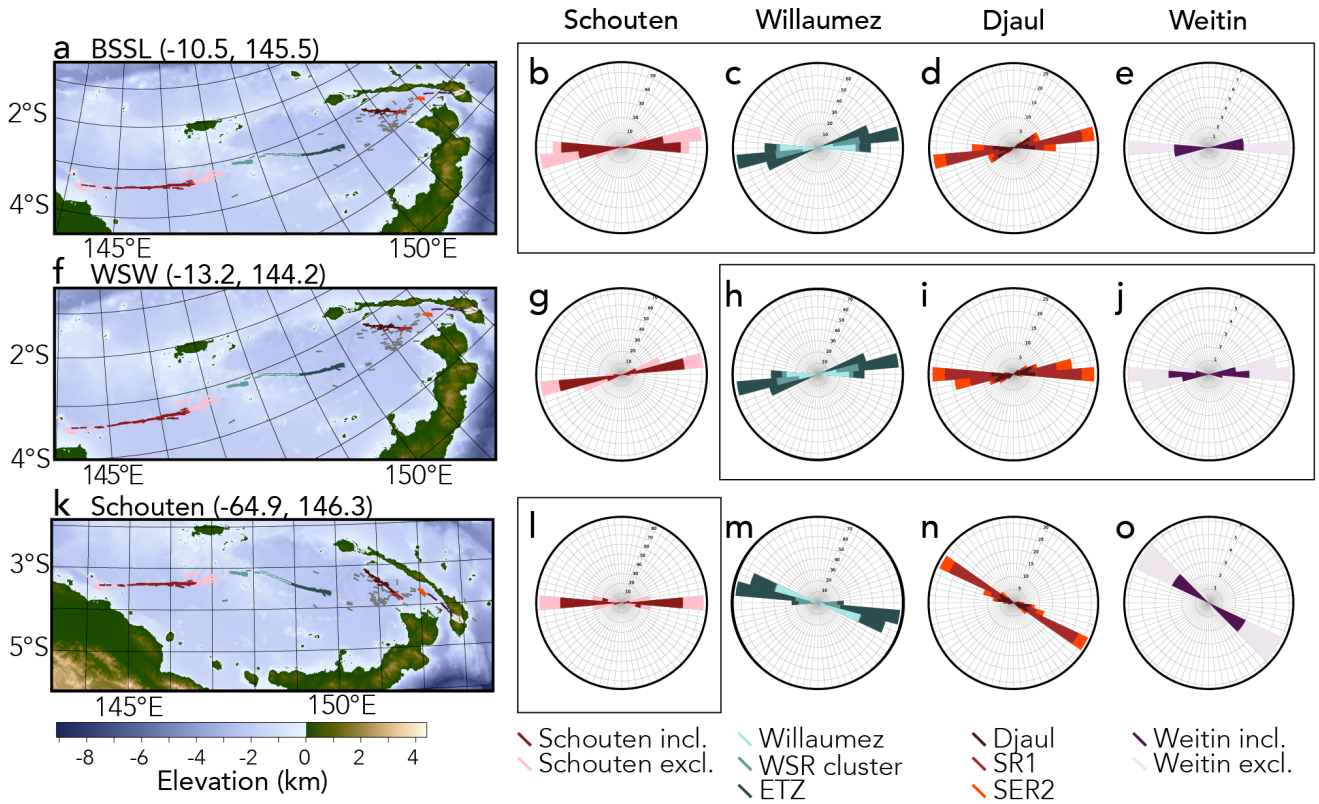

Figure 8 **a**. Oblique Mercator projection (OMP) about the BSSL Euler pole (-10.5°, 145.5°). Nodal-plane strikes of all events are shown and are color coded to match the fault segments on the maps. Other events not shown in any rose diagram are in grey. **b-e**. Rose diagrams in BSSL OMP space for various fault segments. **f**. OMP about the WSW pole (-13.2°, 144.2°). **g-j.** Rose diagrams in WSW OMP space for various fault segments. **k.** OMP about the Schouten pole (-64.9°, 146.3°). WSR: Western Spreading Ridges (see label in Fig. 3a). **l-o.** Rose diagrams in Schouten OMP space for various fault segments. SR1: Southern Rifts, SER2: Southeast Ridges (see labels in Fig. 4a). Those rose diagrams enclosed in boxes are the segments relevant to each pole calculation. Radial grey lines on rose diagrams are at 5° increments.

pected to be fit regardless of being excluded from the calculation.

We found that we can reduce the misfit of the predicted small circles with the earthquake locations along the Schouten by calculating a separate Euler pole for the Schouten segment alone. We calculated (-64.9°, 146.3°) as the Euler pole of best fit, with an RMS error of 1.58 km (Fig. 6, Table 2). Due to the linearity of this fault segment, the Euler pole has a large uncertainty (Table 2); even so, its 95% confidence region does not overlap with our WSW or BSSL poles (Fig. 7). We used the predicted relative motion along the Schouten transform shown in Koulali et al. (2015) to calculate an angular velocity for this pole of 1.41°/Myr. While the uncertainty around this newly derived Euler pole is large, the OMP in Fig. 8k shows that it fits the Schouten well, for the first time producing a linear, east-west striking segment. The nodal-plane strikes are mostly aligned east-west in the middle of the segment. In the rose diagram (Fig. 8l), the majority of nodal-plane strikes plot at 90 or 270°, unlike the Schouten in the other projections shown in Figs 8b and 8g. However, even following our careful event selection process, some of the events have nodal-planes that do not align with the transform, causing a minority of events to plot 10° misaligned on either side. Additionally, in all projections we show (Figs 8a, 8f, 8k) there are some events at the eastern end of the Schouten with nodal-plane strikes that show greater variability and misalignment from east-west. All other transforms along the BSSL have nodal-plane strikes that are not well fit by the Schouten pole. In the Schouten OMP projection, the nodal-plane strikes of events in the Willaumez (Fig. 8m), Djaul (Fig. 8n), and Weitin (Fig. 8o) regions plot in the ranges of 100 to 120°, 110 to 130°, and 130 to 150°, respectively.

4 Discussion

The improved earthquake locations presented here provide the first modern look at seismicity along the BSSL. They allow us to characterize the nature of this plate boundary, including describing which fault segments host seismicity, confirming the aseismic nature of the spreading ridges, and identifying new clusters of seismicity. Locations from standard earthquake catalogs suggest the BSSL is a region with diffuse seismicity (Fig. 1), and better earthquake relocations are needed to better constrain plate boundary zone deformation.

Our results here show that the earthquakes associated with the transforms along the BSSL relocate to localized zones of seismic deformation. In particular, the earthquakes along the Schouten and Willaumez transforms, as well as the western ETZ, relocate to discrete lineations only a few km across (Fig. 2-4), comparable in width to their average horizontal-location uncertainty (~3 km, Table 1) and half the thickness of oceanic crust. We suggest that these segments are well described as finite strike-slip faults rather than zones of distributed deformation and show that the earthquakes on each transform lie on a small circle defined by an Euler pole.

4.1 The Schouten transform

Relocations along the Schouten transform successfully define the zone of seismicity as a narrow region a few kms in width, that widens somewhat east of the extensional jog at 145.95°E. The mechanisms are primarily left-lateral strike-slip, with a few reverse faulting events mainly located close to Papua New Guinea. However, at the eastern end of the Schouten, we also show that the nodal-plane strikes of events are more variable and trend more directly northeast than those on the remainder of the Schouten (Fig. 8k-l). The locations are also more distributed rather than aligned with a feature. We ascribe this complexity to interactions between the termination of the Schouten and the Western Spreading Ridges.

4.2 The Willaumez transform and the ETZ

Along the Willaumez transform, our relocations produce the most linearly aligned, narrow zone of earthquakes along the entire BSSL. They are exclusively left-lateral strike-slip events with no normal or reverse mechanisms. The low horizontal-location uncertainties of the relocations allow us to characterize the ETZ with new precision (Fig. 3). We show that the seismicity of the Willaumez transform and the ETZ behave as an intersection at 149.0°E of two linear segments of different azimuths, which was also shown in the previous OBS work of Eguchi et al. (1986) (see Taylor et al., 1994). Taylor et al. (1994) first described motion along the ETZ as occurring on many faults oriented at 13° to the Willaumez transform, representing Riedel shear motion synthetic to motion on the Willaumez. These Riedel shear faults cut across volcanic fissures on the seafloor. Our OMPs and rose diagrams further support the Riedel geometry of strike-slip motion, as we find an approximately 10° anticlockwise offset in earthquake nodal-planes along the ETZ compared to the Willaumez (Figs 8a, 8c, 8f, 8h), clearly showing that the events along the ETZ cannot be fit with the same Euler pole as the other segments along the BSSL.

4.3 The Djaul and Weitin transforms

Earthquake relocations along the Djaul and Weitin transforms (Fig. 4) succeed in highlighting active fault strands but show more distributed deformation than along either the Schouten or Willaumez transforms. The Djaul is mapped as having two strands which parallel each other for most of its length; our relocations show that this area does have a slightly more diffuse seismicity pattern that may corroborate faulting on both strands. Several events in this region relocate to inside the Manus microplate. They may represent distributed deformation, possibly from bookshelf-style faulting (consistently right-lateral strike-slip on NNE planes), as suggested by Martinez and Taylor (1996).

The focal mechanisms along the Weitin are similarly more distributed in location; while several larger events align well with the fault strand (Fig. 4), a few left-lateral strike slip mechanisms are slightly rotated and relocate farther south of the fault, and there are commonly reverse, oblique reverse, and normal fault mechanisms in this region. One earthquake with a strike-slip mechanism is relocated to south of the Weitin Fault, which we suggest may have occurred on the parallel Sapom Fault. There is a more complex crustal structure in this region due to northward subduction of the Solomon Sea Plate (Cooper and Taylor, 1989), which may lead to the more complex distributed deformation patterns we show in our relocations. It is possible that some of the reverse fault mechanisms we relocate are deeper events which are unrelated to the Weitin transform itself.

4.4 The Adelbert block

The Adelbert block was first suggested by Abers and McCaffrey (1988) and later included in the GPS analysis of Koulali et al. (2015). However, our relocations show that events along this boundary are rare and do not align consistently. Others who have included Adelbert block in their plate models note a much slower displacement along its southeastern boundary, on the order of ~20 mm/yr, compared to the segments of the BSSL (Koulali et al., 2015). Despite extending our catalog search to begin in 1975, we identify just 28 events in this region, only 9 of which relocate successfully and with a high average location uncertainty of 8.41 km (Table 1). A lack of high-resolution seafloor imagery means we cannot map any seafloor fault signatures in this region, though we do note one lineation which may represent a scarp. The relocated events do not define a narrow zone and the nodal-planes are not aligned with the lineation of earthquake locations, both being inconsistent with a simple block boundary. We conclude that an Adelbert block is not well defined, so we do not calculate an Euler pole for these events. However, given our newly derived Euler pole locations and angular velocities for WSW and Schouten, we can perform a three-plate circuit calculation to determine what the corresponding pole and angular velocity for Adelbert-South Bismarck would be if these blocks behaved rigidly. This calculation results in an Adelbert-South Bismarck pole of (-0.84, 144.07, 5.27°/Myr). Such a pole location and rate would predict a high relative motion along the SE Adelbert block boundary (e.g., ~42 mm/yr at -4.5°, 146.0°) which is inconsistent with the level of seismicity observed and the GPS results from Koulali et al. (2015). We infer, therefore, that these blocks are not behaving rigidly.

4.5 Ridge-related seismicity

We confirm previous work that extensional volcanic zones along the BSSL, including the Manus Spreading Center, Western Spreading Ridges, Extensional Transform Zone, Southern Ridges, and Southeast Ridges (Fig. 1), are aseismic at Mw>5 (e.g., Eguchi et al., 1986). We identify almost no events with normal faulting mechanisms along the entire BSSL, except for a few events in the Weitin region (Fig. 4), which is in contrast to the other spreading centers in the region, such as those in the eastern Woodlark Basin, that do host normal as well as strike-slip earthquakes (e.g., Benyshek and Taylor, 2021).

The low location uncertainties of the relocations along the Schouten allow us to identify a sequence of 11 strike-slip earthquakes that occurred in 2019 just north of, and subparallel to, its eastern end (Fig. 2). Although they occur in an area with no high-resolution bathymetry, they appear to cross-cut WSR-parallel and fault-orthogonal seafloor fabric imaged just to the south.

While there are no events with normal-faulting mechanisms that would represent spreading along the volcanic zones, we do relocate some strike-slip events that are associated with them, for example, the cluster of events cross-cutting the Western Spreading Ridges (Fig. 3). These earthquakes align with a lineation on the bathymetry of Auzende et al. (2000), so we provisionally interpret this feature as a strike-slip fault that may act as a conduit for volcanism. It could be a feature like the ETZ which accommodates both extension and strike-slip motion.

A second example of non-extensional ridge seismicity is in the Southern Rifts and Southeast Ridges areas, where we identify strike-slip faulting at the end of each ridge segment (Fig. 4). Two clusters of events that relocate along transform offsets of the Southeast Ridges are included in our pole calculations for the BSSL and WSW sections. They are better fit by the WSW Euler pole than the overall BSSL Euler pole (Fig. 8d,i).

4.6 Plate tectonic interpretation

Several Euler poles have been published to describe the relative motion between the North and South Bismarck Plates (see Table 2; Koulali et al., 2015; Martinez and Taylor, 1996; Tregoning, 2002; Wallace et al., 2004). We use our precisely relocated earthquakes to evaluate these Euler poles and calculate our own best-fit Euler poles. We find that the lowest RMS misfit between pole-predicted small circle segments and the relocated earthquakes along the entire BSSL is for our newly calculated Euler pole at (-10.5°, 145.5°, 7.85°/Myr) (Fig. 6). However, both our Euler pole and all published poles have higher misfits with earthquakes along the Schouten transform specifically, and our OMP visually confirms that this segment is not fit well by the BSSL pole (Fig. 8a).

When fitting the Schouten transform and the other segments with separate Euler poles, we can decrease the average RMS misfit of events along the Schouten with the pole-predicted small circles from 2.07 km to 1.41 km; small circles about this new Euler pole cannot fit the other transform segments (Fig. 8l-o). As Taylor (1979) first proposed, the Schouten transform is not fit well by the same Euler pole as the Willaumez transform and other segments along the BSSL. Furthermore, excluding the Schouten from the BSSL Euler pole calculation gives the WSW pole (-13.2°, 144.2°, 6.02°/Myr), which has a much lower average RMS misfit between the predicted small circles and the relocated earthquakes of 1.18 km for the remainder of the segments. While it is true that our newly derived pole for the Schouten has a high uncertainty (Table 2), we know it is a good fit because the nodal-plane strikes are consistent with the predictions from the Euler pole (Fig. 8). Though the 95% confidence region is large, and overlaps with some previous BSSL pole estimates (Koulali et al., 2015; Tregoning, 2002; Wallace et al., 2004), it is significantly different from the poles we derive here for the BSSL and the WSW segments (Table 2; Fig. 8). We hope that further work taking into account these relocated earthquakes as well as additional (e.g., GPS) constraints will be able to further refine the pole location for the Schouten transform.

That the Schouten transform does not have the same Euler pole as the remainder of the BSSL segments, may either be because of internal deformation of the North and South Bismarck Plates (Taylor, 1979), or the existence of the Adelbert block (Abers and McCaffrey, 1988; Koulali et al., 2015; Wallace et al., 2004), in which case the Schouten would be the boundary between it and the North Bismarck Plate. But the Adelbert block is not well defined: its proposed SE boundary has only minimal seismicity in the entire study range, and the focal mechanisms there do not relocate to a localized region. By introducing an Adelbert block, Koulali et al. (2015) reduced the modeled velocities on Schouten from ~116 mm/yr reported in Tregoning (2002) to ~96 mm/yr. However, the Koulali et al. (2015) data for the two GPS sites that straddle Schouten in the west (TARO and BAMI) imply only 85 mm/yr motion on azimuth 262.7°. Such rapidly varying spatial deformation is not captured well by the proposed Adelbert block model.

Instead, we support the inference of Taylor (1979) that, in order to accommodate the observed motions, there must be some internal plate deformation of the North and South Bismarck Plates between the Schouten transform and the other segments of the BSSL. It is likely that this internal deformation is being accommodated in the Western Spreading Ridges region (Fig. 2), where the St. Andrews Strait hotspot has created a thick crust and weak lithosphere (Fig. 1; Hall and Spakman, 2002; Taylor and Benyshek, 2024). Scattered focal mechanisms that plot in the middle of both the North and South Bismarck Plates and do not relocate along the BSSL show that internal deformation is occurring (Fig. 1; Supplemental Material). In global plate models like Bird (2003), the southwest tip of the Western Spreading Ridges is connected by a transform to the Schouten transform, which would form an unstable triple junction; physiographically, the Western Spreading Ridges terminate south of the Schouten transform fault, within the South Bismarck Plate, again supporting the infer-

ence that internal deformation and non-localized motion is accommodated in this area (see question mark on Figs 6, 7).

We exclude the Djaul transform from our pole calculations because, although it is one of the transform segments of the BSSL, it also borders the Manus microplate and thus may not reliably represent the motion between only the North and South Bismarck Plates. Because we excluded all of these events from our Euler pole calculations, we did not employ our careful selection process to exclude events not along the fault and with misaligned nodal-planes; thus, further analysis of these events may show that the seismicity along the Djaul may indeed be well fit by small circles of both the BSSL and WSW Euler poles, as supported by our OMPs so far (Fig. 8d,i).

4.7 Global significance

The BSSL hosts some of the longest and fastest-slipping oceanic transform faults on Earth, with estimated slip rates ~100mm/yr along some segments (Koulali et al., 2015). Oceanic transform faults are capable of producing great earthquakes (Wiseman and Bürgmann, 2012) which can trigger both local tsunamis (Heidarzadeh et al., 2017) and distant aftershocks (Pollitz et al., 2012). Therefore, understanding the characteristics and distribution of their seismicity is a key aspect in quantifying their hazard. Our results here show that, on the Willaumez and Schouten transforms in particular, seismic activity is tightly localized. Howe et al. (2019) found similar results for the Blanco and Balleny oceanic transform faults using the same relocation procedure. Relocated earthquakes along the 50-km-long G3 strand of the Gofar oceanic transform show similar tight clustering (Wei et al., 2024). The tight clustering of seismicity along oceanic transform faults is in stark contrast to many large-offset continental transform faults such as the San Andreas or Anatolian faults that often have more distributed seismicity and many branching faults (e.g., Ding et al., 2023; Liu et al., 2022). Taken together, this work suggests that oceanic transform faults tend to localize seismicity more effectively than their continental counterparts.

We can also calculate the seismic moment along specific faults and compare these values to what is predicted if the slip is accommodated seismically over a range of depths corresponding to the seismogenic zone, a value otherwise known as the seismic coupling ratio. For the Schouten and Willaumez transforms (excluding the ETZ), we derived summed moment values of 3.3 x 10^{19} and 2.3 x 10^{19} Nm, respectively, for the 20-year observational period. We used only the carefully selected earthquakes included in the pole calculation, so the seismic moment release values might be considered minimum values. We used a shear modulus of 30 GPa (after e.g., Y. Liu et al., 2012) and a seismogenic thickness of 4 km (the average of reported values for oceanic ridge-transform faults, as summarized by Boettcher and Jordan, 2004). For the Schouten and Willaumez transforms, we derived seismic coupling values of 43% and 50%, respectively, based on the fault slip rates reported in Tregoning (2002) and Koulali et al. (2015). These values are significantly higher than average values for oceanic transform faults, which are on the order of 15% (Boettcher and Jordan, 2004). However, a large unknown is the seismogenic width of these faults; the range given by Boettcher and Jordan (2004) is for oceanic ridge-transform faults, and there are no established thermal models of the BSSL that could provide better constraints on these values.

An enigmatic feature of the BSSL is the ETZ, which links the Willaumez Fault with the Manus Spreading Center (Fig. 3). While the Manus ETZ was the first of its kind recognized globally, others were subsequently identified in the Lau Basin, Reykjanes Peninsula and Mak'Arrasou Afar (Taylor et al., 1994; Zellmer and Taylor, 2001). Features typical in ETZ systems globally include en echelon volcanic features and faults that trend at Riedel shear angles to the extension direction (Taylor et al., 1994). In each of these cases, the transforms are seismic, while the volcanic zones are aseismic, at the scale of observation, but it is unknown whether transform fault slip and rifting events are coeval or co-located (e.g., Khodayar et al., 2020). At the Lau Basin ETZ, for example, seismicity is dominated by strike-slip events that do not appear to be associated with magmatic events but rather fault slip (Conder and Wiens, 2011; Eguchi et al., 1989b). Since the spreading along the Manus ETZ is most likely accomplished by subseismic diking events, our work here also cannot resolve whether the strike-slip faulting and spreading along it occur coevally or are partitioned in time.

To resolve this and other open questions, the Bismarck Sea would benefit from additional seafloor surveying, including swath bathymetry and sidescan sonar in targeted regions such as: at the eastern end of the Schouten transform where transform motion is modulated by the WSR; in the middle of the Schouten transform between the Llanes et al. (2009) and Auzende et al. (2000) surveys; just north of the Schouten transform in the 2019 earthquake sequence region; and along the proposed SE Adelbert block boundary. A longer OBS study similar to Eguchi et al. (1986) along the Willaumez transform and ETZ could help disentangle the mechanisms that accommodate extensional transform motion in these zones globally and answer whether spreading events are coeval with strike-slip seismicity or are temporally and spatially partitioned. Finally, full modeling of GPS and mapped fault data, including a separate Schouten transform from the remainder of the BSSL segments, could further refine the Euler poles that we estimate here and additionally clarify the complicated microplate tectonics in this region.

5 Conclusions

The detailed nature of the seismicity along the BSSL has not been determined since its initial discovery and description in 1969. Here, we use a recently developed earthquake relocation method (Howe et al., 2019) to take a modern look at the seismicity along the many segments of this boundary. We find that the left-lateral strike-slip seismicity is localized tightly along the Schouten, Willaumez, Djaul, and Weitin transforms,

and the western ETZ. Several earthquakes that relocate to inside the Manus Microplate may represent distributed deformation by bookshelf-style faulting (right-lateral on NNE-striking planes). We confirm previous work that indicates that the spreading ridges and rifts such as the Western Spreading Ridges, Manus Spreading Center, Southern Rifts, and Southeast Ridges are aseismic at Mw>5; however, we find clusters of strike-slip seismicity at their terminations and cross-cutting them. The strike-slip fault that cross-cuts the volcanic fissures of the ETZ is a synthetic Riedel shear to the adjacent Willaumez transform, with seismicity and focal mechanism nodal-planes aligned 10° counter-clockwise to it. We find that published and our newly calculated North Bismarck – South Bismarck Euler poles do not fit the relocated events along the Schouten transform well; instead, we calculate new Euler poles for the Schouten alone as well as the remainder of the BSSL excluding the Schouten and find that they reduce the RMS misfit of the predicted small circles to the earthquake locations. Since the geometries of the Willaumez and Schouten transforms are inconsistent with a common pole of rotation, we infer that significant internal deformation must occur within the North and South Bismarck Plates. Few earthquakes occur along the SE boundary of the previously proposed Adelbert block and they do not relocate in a tight zone.

6 Acknowledgements

We acknowledge use of data from the Global Seismographic Network (Albuquerque Seismological Laboratory/USGS, 1988; EarthScope Consortium, 1986), Geoscope (Institut de physique du globe de Paris (IPGP) and École et Observatoire des sciences de la Terre de Strasbourg (EOST), 1982), GEOFON (GEOFON Data Centre, 1993), and MedNet (MedNet Project Partner Institutions, 1990) seismic networks. Göran Ekström received support from the Consortium for Monitoring, Technology, and Verification under the Department of Energy National Nuclear Security Administration award number DE-NA0003920. This manuscript was improved by comments from two anonymous reviewers and from editor Matt Wei.

7 Data and code availability

We collected long-period digital seismograms from the Global Seismographic Network (Albuquerque Seismological Laboratory/USGS, 1988; EarthScope Consortium, 1986), Geoscope (Institut de physique du globe de Paris (IPGP) and École et Observatoire des sciences de la Terre de Strasbourg (EOST), 1982), GEOFON (GEOFON Data Centre, 1993), and MedNet (MedNet Project Partner Institutions, 1990) seismic networks.

The relocation algorithm used here is the same version as in Howe et al. (2019) at https://doi.org/10.1093/gji/ggz291. The earthquake data before and after relocation and the code to calculate best-fit small circles is available on Zenodo (Ledeczi et al., 2025).

8 Competing interests

The authors declare no competing interests.

References

Abers, G. and McCaffrey, R. Active deformation in the New Guinea fold-and-thrust belt: Seismological evidence for strike-slip faulting and basement-involved thrusting. *Journal of Geophysical Research: Solid Earth*, 93(B11):13332–13354, 1988. doi: 10.1029/jb093ib11p13332.

Albuquerque Seismological Laboratory/USGS. Global Seismograph Network (GSN - IRIS/USGS), 1988. doi: 10.7914/SN/IU.

Auzende, J.-M., Urabe, T., and Scientific Party. Cruise explores hydrothermal vents of the Manus Basin. *Eos, Transactions American Geophysical Union*, 77(26):244–244, 1996. doi: 10.1029/96eo00174.

Auzende, J.-M., Ishibashi, J.-I., Beaudoin, Y., Charlou, J.-L., Delteil, J., Donval, J.-P., Fouquet, Y., Gouillou, P., Ildefonse, B., Kimura, H., Nishio, Y., Radford-Knoery, J., and Ruellan, E. Rift Propagation and extensive off-axis volcanic and hydrothermal activity in the Manus Basin (Papua New Guinea): MANAUTE Cruise. *International Ridge-Crest Research: Back Arc Basins*, 9(2):21–25, 2000.

Barriga, F., Binns, R., Miller, D., and Herzig, P. *Leg 193 synthesis: Anatomy of an active felsic-hosted hydrothermal system, eastern Manus Basin*. Ocean Drilling Program, 2007. doi: 10.2973/odp.proc.sr.193.2007.

Benyshek, E. K. and Taylor, B. Tectonics of the Papua-Woodlark Region. *Geochemistry, Geophysics, Geosystems*, 22(1), 2021. doi: 10.1029/2020gc009209.

Benyshek, E. K., Taylor, B., and Goodliffe, A. M. A Detailed Reconstruction of the Woodlark Basin. *Geochemistry, Geophysics, Geosystems*, 25(7), 2024. doi: 10.1029/2023gc011410.

Binns, R. A. and Scott, S. D. Actively forming polymetallic sulfide deposits associated with felsic volcanic rocks in the eastern Manus back-arc basin, Papua New Guinea. *Economic Geology*, 88(8):2226–2236, 1993. doi: 10.2113/gsecongeo.88.8.2226.

Bird, P. An updated digital model of plate boundaries. *Geochemistry, Geophysics, Geosystems*, 4(3), 2003. doi: 10.1029/2001gc000252.

Boettcher, M. S. and Jordan, T. H. Earthquake scaling relations for mid-ocean ridge transform faults. *Journal of Geophysical Research: Solid Earth*, 109(B12), 2004. doi: 10.1029/2004jb003110.

Both, R., Crook, K., Taylor, B., Brogan, S., Chappell, B., Frankel, E., Liu, L., Sinton, J., and Tiffin, D. Hydrothermal chimneys and associated fauna in the Manus Back-Arc Basin, Papua New Guinea. *Eos, Transactions American Geophysical Union*, 67(21):489–490, 1986. doi: 10.1029/eo067i021p00489.

Brooks, J. A., Connelly, J. B., Finlayson, D. M., and Wiebenga, W. A. St George's Channel–Bismarck Sea Trough. *Nature Physical Science*, 229(7):205–207, 1971. doi: 10.1038/physci229205a0.

Chen, K., Milliner, C., and Avouac, J. The Weitin Fault, Papua New Guinea, Ruptured Twice by Mw 8.0 and Mw 7.7 Earthquakes in 2000 and 2019. *Geophysical Research Letters*, 46(22):12833–12840, 2019. doi: 10.1029/2019gl084645.

Cleveland, M. and Ammon, C. J. Precise relative earthquake location using surface waves. *Journal of Geophysical Research: Solid Earth*, 118(6):2893–2904, 2013. doi: 10.1002/jgrb.50146.

Conder, J. A. and Wiens, D. A. Shallow seismicity and tectonics of the central and northern Lau Basin. *Earth and Planetary Science Letters*, 304(3–4):538–546, 2011. doi: 10.1016/j.epsl.2011.02.032.

Connelly, J. B. A structural interpretation of magnetometer and seismic profiler records in the Bismarck Sea, Melanesian Archipelago. *Journal of the Geological Society of Australia*, 21 (4):459–469, 1974. doi: 10.1080/00167617408728867.

Connelly, J. B. Tectonic Development of the Bismarck Sea Based on Gravity and Magnetic Modelling. *Geophysical Journal International*, 46(1):23–40, 1976. doi: 10.1111/j.1365-246x.1976.tb01630.x.

Cooper, P. and Taylor, B. Seismotectonics of New Guinea: A model for arc reversal following arc-continent collision. *Tectonics*, 6(1): 53–67, 1987. doi: 10.1029/tc006i001p00053.

Crook, K., Lisitzin, A., and Borissova, I. Results and prospects from the joint USSR Australia USA PNG geological study of the Manus Basin during the 21st cruise of the R/V Akademik Mstislav Keldysh. *Marine Geology Special Issue*, 142(1/4):1–210, 1997.

Denham, D. Distribution of earthquakes in the New Guinea-Solomon Islands Region. *Journal of Geophysical Research*, 74 (17):4290–4299, 1969. doi: 10.1029/jb074i017p04290.

Ding, X., Xu, S., Xie, Y., Van den Ende, M., Premus, J., and Ampuero, J.-P. The sharp turn: Backward rupture branching during the 2023 Mw 7.8 Kahramanmaraş (Türkiye) earthquake. *Seismica*, 2 (3), 2023. doi: 10.26443/seismica.v2i3.1083.

Dziewonski, A. M. and Anderson, D. L. Preliminary reference Earth model. *Physics of the Earth and Planetary Interiors*, 25(4): 297–356, 1981. doi: 10.1016/0031-9201(81)90046-7.

Dziewonski, A. M., Chou, T., and Woodhouse, J. H. Determination of earthquake source parameters from waveform data for studies of global and regional seismicity. *Journal of Geophysical Research: Solid Earth*, 86(B4):2825–2852, 1981. doi: 10.1029/jb086ib04p02825.

EarthScope Consortium. Global Seismograph Network - II, 1986. doi: 10.7914/SN/II.

Eguchi, T., Fujinawa, Y., Ukawa, M., and Bibot, L. Microearthquakes along the back-arc spreading system in the eastern Bismarck Sea. *Geo-Marine Letters*, 6(4):235–240, 1986. doi: 10.1007/bf02239585.

Eguchi, T., Fujinawa, Y., and Ukawa, M. Microearthquakes and tectonics in an active back-arc basin: the Lau Basin. *Physics of the Earth and Planetary Interiors*, 56(3–4):210–229, 1989a. doi: 10.1016/0031-9201(89)90158-1.

Eguchi, T., Fujinawa, Y., Ukawa, M., and Bibot, L. Earthquakes associated with the back-arc opening in the eastern Bismarck Sea: activity, mechanisms, and tectonics. *Physics of the Earth and Planetary Interiors*, 56(3–4):189–209, 1989b. doi: 10.1016/0031-9201(89)90157-x.

Ekström, G., Nettles, M., and Dziewoński, A. The global CMT project 2004–2010: Centroid-moment tensors for 13,017 earthquakes. *Physics of the Earth and Planetary Interiors*, 200–201:1–9, 2012. doi: 10.1016/j.pepi.2012.04.002.

GEBCO Bathymetric Compilation Group. The GEBCO_2023 Grid - a continuous terrain model of the global oceans and land., 2023. doi: 10.5285/F98B053B-0CBC-6C23-E053-6C86ABC0AF7B.

GEOFON Data Centre. GEOFON Seismic Network. GFZ Data Services, 1993. doi: 10.14470/TR560404.

Hall, R. and Spakman, W. Subducted slabs beneath the eastern Indonesia–Tonga region: insights from tomography. *Earth and Planetary Science Letters*, 201(2):321–336, 2002. doi: 10.1016/s0012-821x(02)00705-7.

Hasterok, D., Halpin, J. A., Collins, A. S., Hand, M., Kreemer, C., Gard, M. G., and Glorie, S. New Maps of Global Geological Provinces and Tectonic Plates. *Earth-Science Reviews*, 231: 104069, 2022. doi: 10.1016/j.earscirev.2022.104069.

Heidarzadeh, M., Harada, T., Satake, K., Ishibe, T., and Takagawa, T. Tsunamis from strike-slip earthquakes in the Wharton Basin, northeast Indian Ocean: March 2016 Mw7.8 event and its relationship with the April 2012 Mw 8.6 event. *Geophysical Journal International*, 211(3):1601–1612, 2017. doi: 10.1093/gji/ggx395.

Hohnen, P. *Geology of New Ireland*. Bureau of Mineral Resources Australia, 1970.

Howe, M., Ekström, G., and Nettles, M. Improving relative earthquake locations using surface-wave source corrections. *Geophysical Journal International*, 219(1):297–312, 2019. doi: 10.1093/gji/ggz291.

Institut de physique du globe de Paris (IPGP) and École et Observatoire des sciences de la Terre de Strasbourg (EOST). GEOSCOPE, French Global Network of broad band seismic stations, 1982. doi: 10.18715/GEOSCOPE.G.

Johnson, R., Smith, I., and Taylor, S. Hot-spot volcanism in St. Andrew Strait, Papua New Guinea: Geochemistry of a bimodal rock suite, 1978.

Johnson, R., Mutter, J., and Arculus, R. Origin of the Willaumez-Manus Rise, Papua New Guinea. *Earth and Planetary Science Letters*, 44(2):247–260, 1979. doi: 10.1016/0012-821x(79)90173-0.

Johnson, T. and Molnar, P. Focal mechanisms and plate tectonics of the southwest Pacific. *Journal of Geophysical Research*, 77 (26):5000–5032, 1972. doi: 10.1029/jb077i026p05000.

Joseph, D., Taylor, B., Shor, A. N., and Yamazaki, T. *The Nova-Canton Trough and the Late Cretaceous evolution of the central Pacific*, page 171–185. American Geophysical Union, 1993. doi: 10.1029/gm077p0171.

Khodayar, M., Björnsson, S., Víkingsson, S., and Jónsdóttir, G. S. Unstable Rifts, a Leaky Transform Zone and a Microplate: Analogues from South Iceland. *Open Journal of Geology*, 10(04): 317–367, 2020. doi: 10.4236/ojg.2020.104017.

Koulali, A., Tregoning, P., McClusky, S., Stanaway, R., Wallace, L., and Lister, G. New Insights into the present-day kinematics of the central and western Papua New Guinea from GPS. *Geophysical Journal International*, 202(2):993–1004, 2015. doi: 10.1093/gji/ggv200.

Ledeczi, A., Ekström, G., and Taylor, B. Earthquake Relocations Illuminate Tectonics along the Bismarck Sea Seismic Lineation, Papua New Guinea, 2025. doi: 10.5281/ZENODO.14941399.

Lee, S.-M. and Ruellan, E. *Tectonic and magmatic evolution of the Bismarck Sea, Papua New Guinea: Review and new synthesis*, page 263–286. American Geophysical Union, 2006. doi: 10.1029/166gm14.

Liu, Y., McGuire, J. J., and Behn, M. D. Frictional behavior of oceanic transform faults and its influence on earthquake characteristics. *Journal of Geophysical Research: Solid Earth*, 117(B4), 2012. doi: 10.1029/2011jb009025.

Liu, Y.-K., Ross, Z. E., Cochran, E. S., and Lapusta, N. A unified perspective of seismicity and fault coupling along the San Andreas Fault. *Science Advances*, 8(8), 2022. doi: 10.1126/sciadv.abk1167.

Llanes, P., Silver, E., Day, S., and Hoffman, G. Interactions between a transform fault and arc volcanism in the Bismarck Sea, Papua New Guinea. *Geochemistry, Geophysics, Geosystems*, 10 (6), 2009. doi: 10.1029/2009gc002430.

Macpherson, C. G., Hilton, D. R., Sinton, J. M., Poreda, R. J., and Craig, H. High 3He/4He ratios in the Manus backarc basin: Implications for mantle mixing and the origin of plumes in the western Pacific Ocean. *Geology*, 26(11):1007, 1998. doi: 10.1130/0091-7613(1998)026<1007:hhhrit>2.3.co;2.

Martinez, F. and Taylor, B. Backarc spreading, rifting, and microplate rotation, between transform faults in the Manus Basin.

Marine Geophysical Researches, 18(2–4):203–224, 1996. doi: 10.1007/bf00286078.

Martinez, F. and Taylor, B. Controls on back-arc crustal accretion: insights from the Lau, Manus and Mariana basins. *Geological Society, London, Special Publications*, 219(1):19–54, 2003. doi: 10.1144/gsl.sp.2003.219.01.02.

McClusky, S., Mobbs, K., Stolz, A., Barsby, D., Loratung, W., Lambeck, K., and Morgan, P. The Papua New Guinea Satellite Crustal Motion Surveys. *Australian Surveyor*, 39(3):194–214, 1994. doi: 10.1080/00050328.1994.10558445.

MedNet Project Partner Institutions. Mediterranean Very Broadband Seismographic Network (MedNet), 1990. doi: 10.13127/SD/FBBBTDTD6Q.

Pollitz, F. F., Stein, R. S., Sevilgen, V., and Bürgmann, R. The 11 April 2012 east Indian Ocean earthquake triggered large aftershocks worldwide. *Nature*, 490(7419):250–253, 2012. doi: 10.1038/nature11504.

Ripper, I. Earthquake focal mechanisms in the New Guinea/-Solomon Islands region, 1975a.

Ripper, I. Part 6. Present plate boundary seismic, volcanic and kinematic processes: Seismicity and earthquake focal mechanisms in the New Guinea Solomon Islands region. *Exploration Geophysics*, 6(2):80–81, 1975b. doi: 10.1071/eg975080.

Sinton, J., Liu, L., Taylor, B., and Chappell, B. Petrology, magmatic budget and tectonic setting of Manus back-arc basin lavas. *EOS (Trans. Am. Geophys. Union)*, 67:377–378, 1986.

Sinton, J. M. Magma Genesis and Mantle Heterogeneity in the Manus Back-Arc Basin, Papua New Guinea. *Journal of Petrology*, 44(1):159–195, 2003. doi: 10.1093/petrology/44.1.159.

Smith, G. P. and Ekström, G. Improving teleseismic event locations using a three-dimensional Earth model. *Bulletin of the Seismological Society of America*, 86(3):788–796, 1996. doi: 10.1785/bssa0860030788.

Taylor, B. The tectonics of the Bismarck Sea region [B.Sc. Honors Thesis], 1975.

Taylor, B. Bismarck Sea: Evolution of a back-arc basin. *Geology*, 7(4):171, 1979. doi: 10.1130/0091-7613(1979)7<171:bseoab>2.0.co;2.

Taylor, B. and Benyshek, E. K. Oceanic Plateau and Spreading Ridge Subduction Accompanying Arc Reversal in the Solomon Islands. *Geochemistry, Geophysics, Geosystems*, 25(1), 2024. doi: 10.1029/2023gc011270.

Taylor, B., Crook, K., and Sinton, J. Fast Spreading and Sulfide Deposition in Manus Back-Arc Basin. *AAPG Bulletin*, 70, 1986.

Taylor, B., Crook, K., Sinton, J., and Petersen, L. Manus Basin, Papua New Guinea, SeaMARC II Sidescan Sonar Imagery (Sheets 1-3) and Bathymetry (Sheets 4-6), 1:250,000. In *Pacific Seafloor Atlas*, page 1–3. Hawaii Institute of Geophysics, 1991.

Taylor, B., Crook, K., and Sinton, J. Extensional transform zones and oblique spreading centers. *Journal of Geophysical Research: Solid Earth*, 99(B10):19707–19718, 1994. doi: 10.1029/94jb01662.

Tregoning, P. Plate kinematics in the western Pacific derived from geodetic observations. *Journal of Geophysical Research: Solid Earth*, 107(B1), 2002. doi: 10.1029/2001jb000406.

Tregoning, P., Jackson, R. J., McQueen, H., Lambeck, K., Stevens, C., Little, R. P., Curley, R., and Rosa, R. Motion of the South Bismarck Plate, Papua New Guinea. *Geophysical Research Letters*, 26(23):3517–3520, 1999.

Tufar, W. Modern Hydrothermal Activity, Formation of Complex Massive Sulfide Deposits and Associated Vent Communities in the Manus Back-Arc Basin (Bismarck Sea, Papua New Guinea. *Mitt Österr. Geol. Ges*, 82, 1990.

Wallace, L. M., Stevens, C., Silver, E., McCaffrey, R., Loratung, W., Hasiata, S., Stanaway, R., Curley, R., Rosa, R., and Taugaloidi, J. GPS and seismological constraints on active tectonics and arc-continent collision in Papua New Guinea: Implications for mechanics of microplate rotations in a plate boundary zone. *Journal of Geophysical Research: Solid Earth*, 109(B5), 2004. doi: 10.1029/2003jb002481.

Wallace, L. M., McCaffrey, R., Beavan, J., and Ellis, S. Rapid microplate rotations and backarc rifting at the transition between collision and subduction. *Geology*, 33(11):857, 2005. doi: 10.1130/g21834.1.

Wei, M., He, L., and Smith-Konter, B. A model of the earthquake cycle along the Gofar oceanic transform faults. *Seismica*, 3(2), 2024. doi: 10.26443/seismica.v3i2.1382.

Wiseman, K. and Bürgmann, R. Stress triggering of the great Indian Ocean strike-slip earthquakes in a diffuse plate boundary zone. *Geophysical Research Letters*, 39(22), 2012. doi: 10.1029/2012gl053954.

Zellmer, K. E. and Taylor, B. A three-plate kinematic model for Lau Basin opening. *Geochemistry, Geophysics, Geosystems*, 2(5), 2001. doi: 10.1029/2000gc000106.